

# **Determination of the beam asymmetry $\Sigma$ in $\eta$ - and $\eta'$ -photoproduction using Bayesian statistics**

JAKOB MICHAEL KRAUSE

Masterarbeit in Physik  
angefertigt im Helmholtz-Institut für Strahlen- und  
Kernphysik

vorgelegt der  
Mathematisch-Naturwissenschaftlichen Fakultät  
der  
Rheinischen Friedrich-Wilhelms-Universität  
Bonn

Sep 2022

DRAFT

I hereby declare that this thesis was formulated by myself and that no sources or tools other than those cited were used.

Bonn, .....  
Date

.....  
Signature

- 1. Gutachterin: JUN. PROF. DR. ANNIKA THIEL
- 2. Gutachter: PROF. DR. JOCHEN DINGFELDER

DRAFT

# Contents

---

<b>1</b>	<b>Introduction</b>	<b>1</b>
1.1	Photoproduction of Pseudoscalar Mesons . . . . .	4
1.2	Measurement of Polarization Observables . . . . .	5
1.3	Introduction to BAYESIAN statistics . . . . .	5
1.3.1	Frequentist Approach . . . . .	5
1.3.2	Bayesian approach . . . . .	5
1.3.3	Combining inferences . . . . .	5
1.4	Motivation and Structure of this Thesis . . . . .	5
<b>2</b>	<b>Experimental Setup</b>	<b>7</b>
2.1	Production of (polarized) high energy photon beam . . . . .	7
2.1.1	Tagger . . . . .	8
2.2	Beam Target . . . . .	8
2.3	Calorimeters . . . . .	8
2.4	Trigger . . . . .	8
<b>3</b>	<b>Event selection</b>	<b>11</b>
3.1	Reconstruction of events . . . . .	12
3.2	Preselection and charge cut . . . . .	12
3.3	Time of particles . . . . .	13
3.4	Kinematic constraints . . . . .	15
3.4.1	Derivation of cut conditions . . . . .	15
3.4.2	Determination of cut ranges . . . . .	16
3.4.3	Quality of event selection . . . . .	21
3.5	Investigation of background and additional cuts . . . . .	23
3.5.1	Inspecting plausibility of background reactions . . . . .	24
3.5.2	Misidentification of background reactions . . . . .	26
3.5.3	Examination of additional cuts . . . . .	31
3.6	Summary of event selection . . . . .	34
3.6.1	Reaction $\gamma p \rightarrow p\eta' \rightarrow p\gamma\gamma$ . . . . .	34
3.6.2	Reaction $\gamma p \rightarrow p\eta \rightarrow p\gamma\gamma$ . . . . .	35
<b>4</b>	<b>Extraction of the beam asymmetries <math>\Sigma_\eta</math> and <math>\Sigma_{\eta'}</math></b>	<b>37</b>
4.1	Methods . . . . .	38
4.1.1	Event yield asymmetries . . . . .	38
4.1.2	Event based fit . . . . .	41

4.2	Determination of $\Sigma_\eta$ using Bayesian statistics . . . . .	44
4.2.1	Application of methods to toy Monte Carlo data . . . . .	44
4.2.2	Application of methods to data . . . . .	53
4.2.3	Discussion . . . . .	56
4.3	Determination of $\Sigma_{\eta'}$ . . . . .	58
4.3.1	Application of event based fit to toy Monte Carlo data . . . . .	58
4.3.2	Application of event based fit to data . . . . .	64
4.3.3	Systematic error . . . . .	68
<b>5</b>	<b>Discussion of results</b>	<b>73</b>
5.1	Comparison of results to existing data . . . . .	73
5.2	Comparison of results to PWA calculations . . . . .	75
5.3	Final discussion of methods . . . . .	75
<b>5</b>	<b>Summary and outlook</b>	<b>73</b>
<b>A</b>	<b>Additional plots and calculations</b>	<b>75</b>
A.1	Statistical error for the asymmetry $A(\phi)$ . . . . .	75
A.2	Kinematic variables for each bin . . . . .	76
A.2.1	Coplanarity . . . . .	76
A.2.2	Polar angle difference . . . . .	76
A.2.3	Missing mass . . . . .	76
A.2.4	Invariant mass . . . . .	76
<b>B</b>	<b>Discussion of binned fits</b>	<b>77</b>
<b>C</b>	<b>Investigation of truncated posteriors</b>	<b>79</b>
	<b>Bibliography</b>	<b>81</b>
	<b>List of Figures</b>	<b>83</b>
	<b>List of Tables</b>	<b>89</b>



## Discussion of results

This chapter will present a discussion of results for the beam asymmetry  $\Sigma$  in the reaction  $\gamma p \rightarrow p\eta' \rightarrow p\gamma\gamma$  obtained with the CBELSA/TAPS experiment. No dedicated discussion of the results obtained for  $\eta$  photoproduction will be given here. Very good agreement between the results for  $\Sigma_\eta$  in this work and reference [Afz19] makes this obsolete, because the findings for  $\Sigma_\eta$  compared to various previous measurements and existing PWA predictions are discussed in reference [Afz19] in detail. However, final remarks regarding the used fitting methods will be made after the results for  $\Sigma_{\eta'}$  obtained in this thesis were compared to existing data, and as a next step compared to existing PWA model predictions.

### 5.1 Comparison of results to existing data

The data situation for any observables in  $\eta'$  photoproduction is scarce because on one hand the production cross section is very small while on the other hand high center of mass energies are needed to observe the reaction  $\gamma p \rightarrow p\eta'$ . To collect sufficient statistics at these energies, very high energetic photon beams are necessary because the photon beam Intensity  $I(E_\gamma)$  approximately behaves like [Leo94]

$$I(E_\gamma) \propto \frac{1}{E_\gamma}. \quad (5.1)$$

Next to a measurement of the beam asymmetry in  $\eta'$  photoproduction near threshold at GrAAL [Lev+14], there exists one other recent measurement of  $\Sigma_{\eta'}$  at CLAS [Col+17]. In this work the beam asymmetry could be extracted covering the beam energy range of  $1500 \text{ MeV} \leq E_\gamma < 1800 \text{ MeV}$  and is binned as  $(\Delta E_\gamma, \Delta \cos \theta) = (100 \text{ MeV}, 0.33)$ . Thus, only the results from reference [Col+17] are suited for comparison which are binned as  $(\Delta E_\gamma, \Delta \cos \theta) = (54 \text{ MeV}, 0.2)$ . Of all kinematic bins provided by reference [Col+17] only energy bins where the bin centers approximately align with the energy bins chosen in this thesis are considered for further investigation. Figure 5.1 shows the results for the beam asymmetry  $\Sigma_{\eta'}$  compared with results reported by [Col+17]. First of all, one may notice the large difference in statistical errors between the two datasets. This can be explained by considering that the results obtained by COLLINS ET AL. [Col+17] were extracted via the charged decay  $\eta' \rightarrow \pi^+\pi^-\eta \rightarrow 2\pi^+2\pi^-\pi^0$  with a branching ratio of  $\text{BR} = 42.6 \cdot 22.02\% = 9.38\%$  [Wor+22] as

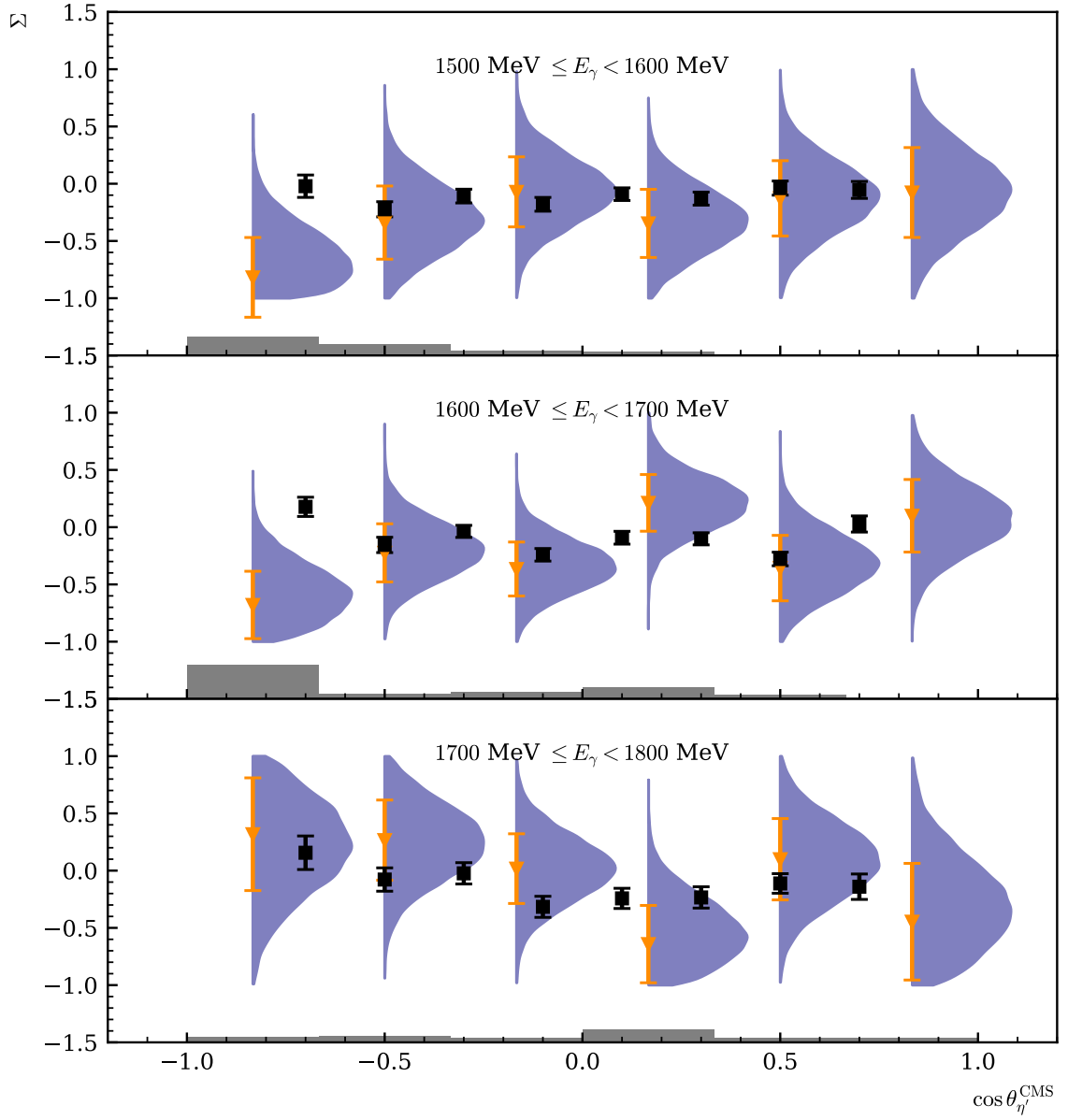


**Figure 5.1:** Results for the beam asymmetry  $\Sigma_{\eta'}$  (orange errorbars and distributions) compared with the results for the energy bins  $E_\gamma = 1569 \text{ MeV}$ ,  $E_\gamma = 1676 \text{ MeV}$ ,  $E_\gamma = 1729 \text{ MeV}$  reported in reference [Col+17] (black errorbars). Systematical errors are shown as grey bars.



opposed to the neutral decay  $\eta' \rightarrow \gamma\gamma$  with a branching ratio of  $\text{BR} = 2.2\%$ . [Wor+22]. Furthermore, the electrons impinging on the radiator target at CLAS were accelerated to 4.5 GeV [Col+17], increasing the statistics in the photon beam energy range of interest compared with CBELSA/TAPS data, where the electrons are only accelerated to 3.5 GeV. Aside from the large difference in statistical errors, generally good agreement between the two datasets exists. Most datapoints are compatible within their statistical errors and the angular profile of the beam asymmetry is displayed equivalently. The largest discrepancy between both datasets exists in backwards direction for the first two energy bins; although the angular bins do not exactly match it is noteworthy that there is a sign flip between the different measurements that can not be accounted for by combined statistical and systematical error (for the CLAS measurement a systematic error due to the determination of the photon beam polarization of 6% is reported [Col+17]). It is not understood why these bins show this particular behavior as no indication towards any additional systematic effects has been found. Note however that without identical binning only vague conclusions regarding the agreement of both datasets can be made. The given datasets allow to identify that there is in general consistency and no large unaccounted systematic uncertainties. Direct comparability can only be achieved if statistics at high center of mass energies are increased.

Due to the placement of the coherent edge the beam asymmetry  $\Sigma_{\eta'}$  could be extracted at beam energies up to  $E_\gamma = 1800$  MeV in this work although the CBELSA/TAPS experiment theoretically provides photon beam energies of maximally  $E_\gamma^{\text{max}} = 3200$  MeV. Yet, the event yield included less than  $10^4$  events collected in roughly four months of beam time. Next to small cross section and branching ratio to a neutral final state this illustrates the effect of Eq. 5.1 during data collection leading to large statistical errors and background contributions when determining the beam asymmetry. Furthermore only a coarse binning in  $(E_\gamma, \cos \theta)$  could be chosen to account for the available statistics, denying a detailed investigation of the beam asymmetry  $\Sigma_{\eta'}(E_\gamma, \cos \theta)$ . In order to collect more statistics at high beam energies in future beam times of the CBELSA/TAPS experiment, e.g. to further investigate the reaction  $\gamma p \rightarrow p\eta'$ , either longer beam times and/or shifting the coherent edge towards higher energies should be considered. Also, the decay channel  $\eta' \rightarrow \pi^0 \pi^0 \eta$  may be investigated to increase precision of the existing data.

## 5.2 Comparison of results to PWA calculations

Figure 5.2 shows the new results for the beam asymmetry  $\Sigma$  in  $\eta'$  photoproduction obtained with the CBELSA/TAPS experiment compared with existing PWA-predictions. Shown is the etaMAID2018 solution [Tia+18], which already included results from the measurements [Col+17] and [Lev+14] in the fit. This however puts bias towards the fitted data on the PWA solution such that the same remarks regarding agreement of the results of this thesis and the PWA calculations can be made as in the previous section; generally the obtained data points are described well by the PWA predictions with the exception of the backwards direction at the first two energy bins. This indicates that the previous measurements of  $\Sigma_{\eta'}$  had a large influence on the PWA fits, especially when considering that before these measurements were added, the PWA solutions failed to describe the beam asymmetry in  $\eta'$  photoproduction, generally showing the wrong sign [Col+17]. Thus, similarly to the previous section, only a vague conclusion of general agreement between data points and PWA solutions can be drawn.

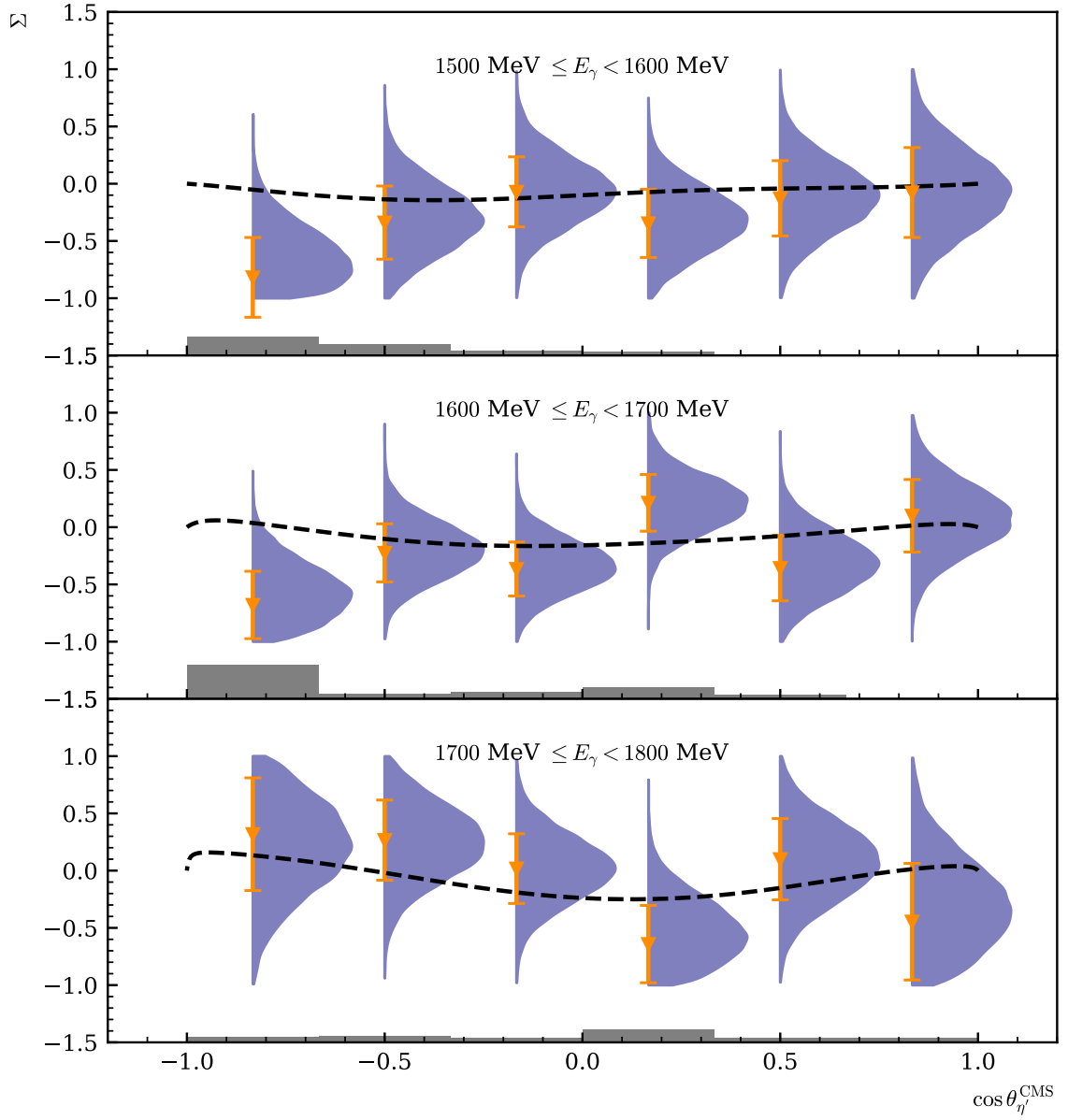


**Figure 5.2:** Results for the beam asymmetry  $\Sigma_{\eta'}$  (orange errorbars and distributions) compared with PWA solutions: etaMAID [Tia+18](dashed black line),... The errorbars only depict statistical error, the systematic error is shown as grey bars.

## **5.3 Final discussion of methods**



# Bibliography

---

- [Afz19] F. N. Afzal, *Measurement of the beam and helicity asymmetries in the reactions  $\gamma p \rightarrow p\pi^0$  and  $\gamma p \rightarrow p\eta$* , PhD thesis: Rheinische Friedrich-Wilhelms-Universität Bonn, 2019, URL: <https://hdl.handle.net/20.500.11811/8064> (cit. on p. 73).
- [Leo94] W. R. Leo, *Techniques for Nuclear and Particle Physics Experiments, A How-to Approach*, vol. 2, Springer-Verlag Berlin Heidelberg GmbH, 1994 (cit. on p. 73).
- [Lev+14] P. Levi Sandri et al., *First Measurement of the  $\Sigma$  Beam Asymmetry in  $\eta'$  Photoproduction off the Proton near Threshold*, (2014) (cit. on pp. 73, 75).
- [Col+17] P. Collins et al., *Photon beam asymmetry  $\Sigma$  for  $\eta$  and  $\eta'$  photoproduction from the proton*, Physics Letters B (2017) (cit. on pp. 73–75).
- [Wor+22] R. L. Workman et al., *Review of Particle Physics*, PTEP **2022** (2022) 083C01 (cit. on pp. 73, 75).
- [Tia+18] L. Tiator et al., *Eta and etaprime photoproduction on the nucleon with the isobar model EtaMAID2018*, The European Physical Journal A **54** (2018), URL: <https://doi.org/10.1140%2Fepja%2Fi2018-12643-x> (cit. on pp. 75, 76).



# List of Figures

---

1.1	Running coupling of QCD. The colored data points represent different methods to obtain a value for $\alpha_s$ . For more details it may be referred to [Wor+22]. . . . .	2
1.2	Calculated nucleon (isospin $I = 1/2$ ) resonances compared to measurements. Left in each column are the calculations [ <b>bonnmodel</b> ], the middle shows the measurements and PDG rating [Wor+22] . . . . .	3
1.3	FEYNMAN diagram for the s-channel photoproduction of pseudoscalar mesons, adapted from [Afz19] . . . . .	4
2.1	[ <b>cb</b> ] . . . . .	7
2.2	[ <b>cb</b> ] . . . . .	8
2.3	[ <b>cb</b> ] . . . . .	8
2.4	D. WALTHER in [ <b>urban</b> ] . . . . .	9
2.5	[ <b>cb</b> ] . . . . .	9
2.6	[ <b>cb</b> ] . . . . .	10
3.1	Distribution of event classes in $\eta' \rightarrow \gamma\gamma$ production . . . . .	13
3.2	Time information of all final state particles and the beam photon for 3PED $\eta'$ production . . . . .	14
3.3	Reaction time $t_r$ for 3PED and 2.5PED $\eta'$ production. The yellow region indicate the sidebands while the purple colored interval is the selected prompt peak. . . . .	15
3.4	Coplanarity of the $p\eta'$ final state with all other cuts applied for the energy bin $1500 \text{ MeV} \leq E_\gamma < 1600 \text{ MeV}$ . The vertical dashed lines show the cut ranges obtained from a gaussian fit to the data (open circles). The solid black histograms represent fitted MC data of $\eta' \rightarrow \gamma\gamma$ . . . . .	19
3.5	Polar angle difference of the $p\eta'$ final state with all other cuts applied for the energy bin $1500 \text{ MeV} \leq E_\gamma < 1600 \text{ MeV}$ . The vertical dashed lines show the cut ranges obtained from a gaussian fit to the data (open circles). The solid black histograms represent fitted MC data of $\eta' \rightarrow \gamma\gamma$ . . . . .	20
3.6	Missing mass of the $p\eta'$ final state with all other cuts applied for the energy bin $1500 \text{ MeV} \leq E_\gamma < 1600 \text{ MeV}$ . The vertical dashed lines show the cut ranges obtained from a fit to data (open circles) employing a Novosibirsk function. The solid colored histograms represent fitted MC data from relevant photoproduction reactions: in black $\eta'$ , in green $\pi^0$ , in red $\eta$ , in blue $\omega$ , in yellow $2\pi^0$ , magenta $\pi^0\eta$ . The turquoise histogram is the sum of all MC histograms. . . . .	21

3.7	Invariant mass of the $p\eta'$ final state with all other cuts applied for all energy and angular bins. The open circles represent the measured data, the solid colored histograms fitted MC data from relevant photoproduction reactions: in black $\eta'$ , in green $\pi^0$ , in red $\eta$ , in blue $\omega$ , in yellow $2\pi^0$ and in magenta $\pi^0\eta$ . The turquoise histogram is the sum of all MC histograms. . . . .	22
3.8	Invariant mass of the $p\eta'$ final state with all other cuts applied for the energy bin $1500 \text{ MeV} \leq E_\gamma < 1600 \text{ MeV}$ . The vertical dashed lines show the cut ranges obtained from a gaussian fit to the $\eta'$ MC data (solid black histogram). The open circles represent the measured data, the solid colored histograms fitted MC data from relevant photoproduction reactions: in black $\eta'$ , in green $\pi^0$ , in red $\eta$ , in blue $\omega$ , in yellow $2\pi^0$ and in magenta $\pi^0\eta$ . The turquoise histogram is the sum of all MC histograms. . . .	22
3.9	Acceptance for the reaction $\gamma p \rightarrow p\eta'$ after all cuts that have been discussed so far for 2.5PED and 3PED events . . . . .	23
3.10	Fraction of background events in the analyzed beam energy and angular bins. . . . .	24
3.11	Acceptance for possible background contributions . . . . .	25
3.12	Generated energies of $\gamma_3$ and $\gamma_4$ in $2\pi^0$ and $\pi^0\eta$ photoproduction MC data. The threshold of 20 MeV is marked by a vertical red line. $E_{\gamma_4}$ is shown on the top, $E_{\gamma_3}$ is shown on the bottom of each figure. . . . .	28
3.13	$E_\gamma^{\text{gen}}$ vs. $E_\gamma^{\text{rec}}$ of $\gamma_1$ and $\gamma_2$ for $2\pi^0$ (top) and $\pi^0\eta$ (bottom) production. The slope $E_\gamma^{\text{gen}} = E_\gamma^{\text{rec}}$ is marked by a solid line. . . . .	29
3.14	Polar angle difference $\Delta\theta$ between $\gamma_2$ and $\gamma_3$ of the $\pi^0\eta$ final state. . . . .	30
3.15	Illustration of the misidentification process during reconstruction. Enumeration of photons is now arbitrary. . . . .	30
3.16	Generated CMS angle $\cos\theta_{\text{gen}}$ vs. reconstructed CMS angle $\cos\theta_{\text{rec}}$ for both background reactions. The slope $\cos\theta_{\text{gen}} = \cos\theta_{\text{rec}}$ is indicated by the solid line. . .	31
3.17	Detector hits of the recoil proton, as obtained from MC data for the production of $\eta'$ , $2\pi^0$ and $\pi^0\eta$ . CB: Crystal Barrel, FW: forward dector, MT: MiniTAPS . . . . .	33
3.18	Difference in measured and calculated beam energy. Data points are shown as open circles, MC data as solid histograms: in black $\eta'$ , in green $\pi^0$ , in red $\eta$ , in blue $\omega$ , in yellow $2\pi^0$ and in magenta $\pi^0\eta$ . The turquoise histogram is the sum of all MC histograms. . . . .	34
3.19	Invariant mass spectrum passing different stages in the event selection process. In the end clear peaks for all possibly produced mesons are visible. The vertical lines indicate the mean cut ranges over all energy and angle bins. . . . .	35
3.20	Invariant mass spectrum passing different stages in the event selection process. In the end clear peaks for all possibly produced mesons are visible. Taken from [Afz19]. . .	36
4.1	Left: Definition of angles $\alpha, \phi, \varphi$ . Right: Photon momentum $\vec{k}$ and polarization $\vec{\epsilon}$ define the beam polarization plane while the reaction plane is defined by the recoil proton $p$ and produced meson $M$ . . . . .	37



- 4.2 Posterior predictive checks  $p(A_{\text{rep}}|A)$  from a BAYESIAN fit to the event yield asymmetries for six toy Monte Carlo bins are shown as distributions. The data points in the upper plot are the asymmetry  $A(\phi)$ , which was additionally fitted using a  $\chi^2$  fit (solid line). The goodness of fit is shown using  $p$ -values, which give the fraction  $T(A_{\text{rep}} > A)$  of replicated samples greater than the original measured value, with propagated statistical error bars on the bottom of each plot. The expected mean value of  $T(A_{\text{rep}} > A) = 0.5$  is indicated by the dashed line. . . . . 46
- 4.3  $p$  values of all toy Monte Carlo bins. They are centered around their mean at 0.5, which is indicated by the dashed line, and show no bias towards higher or lower values, thus confirming an adequate fit. . . . . 47
- 4.4 Left: Combined posterior distributions of all 10000 fits normalized by their respective standard deviation. Right: Unaltered combined posterior distributions of all 10000 fits. A GAUSSIAN fit was performed to determine mean  $\mu$  and standard deviation  $\sigma$  of the distributions with results given on top. . . . . 47
- 4.5 Left: relative error  $\frac{\sigma_{\text{MCSE}}}{\text{median}[p(\Sigma|y)]}$  Right:  $\hat{R}$  associated with the fit parameter  $\Sigma$ . Both are shown for all 10000 fits. The critical values that should not be exceeded are marked by dashed lines. . . . . 48
- 4.6 Combined posteriors for the beam asymmetries  $\Sigma$  and  $\Sigma^{\text{bkg}}$  from all 1000 event based fits. Left: Residuals  $\Xi$  Right: Unnormalized posterior distributions. A GAUSSIAN fit is performed on the distributions with results for mean  $\mu$  and standard deviation  $\sigma$  on top. 50
- 4.7 Combined posterior probabilities using the *pooled likelihood* approach. Left: Signal beam asymmetry, Right: background beam asymmetry. Mean and standard deviation as obtained from a Gaussian fit are shown on top . . . . . 51
- 4.8 Left: relative error  $\frac{\sigma_{\text{MCSE}}}{\text{median}[p(\Sigma|y)]}$  Right:  $\hat{R}$  associated with the fit parameter  $\Sigma$ . Both are shown for all 1000 fits. The critical values that should not be exceeded are marked by dashed lines. . . . . 51
- 4.9 Posterior predictive check using the draws of the detector coefficients  $a$  and  $b$ . Points with error bars are the polarization weighted sum of event yields. The dashed line is the mean of the predictive values while the solid opaque lines are representative of one simulation draw  $a^{(s)}, b^{(s)}$ . . . . . 52
- 4.10 Posterior predictive checks  $p(A_{\text{rep}}|A)$  from a BAYESIAN fit to the event yield asymmetries for all angular bins of the energy bin  $1250 \text{ MeV} \leq E_\gamma < 1310 \text{ MeV}$ . The data points in the upper plot are the asymmetry  $A(\phi)$ , which was additionally fitted using a  $\chi^2$  fit (solid line). The goodness of fit is shown using  $p$ -values, which give the fraction  $T(A_{\text{rep}} > A)$  of replicated samples greater than the original measured value, with propagated statistical error bars on the bottom of each plot. The expected mean value of  $T(A_{\text{rep}} > A) = 0.5$  is indicated by the dashed line. . . . . 54
- 4.11  $p$  values generated using all fits. They are centered around their mean at 0.5, which is indicated by the dashed line, and show no bias towards higher or lower values, thus confirming an adequate fit. . . . . 55
- 4.12 Left: relative error  $\frac{\sigma_{\text{MCSE}}}{\text{median}[p(\Sigma|y)]}$  Right:  $\hat{R}$  associated with the fit parameter  $\Sigma$ . Both are shown for all  $11 \cdot 12$  binned fits to the asymmetry  $A(\phi)$ . The critical values that should not be exceeded are marked by dashed lines. . . . . 55

4.13	Left: relative error $\frac{\sigma_{\text{MCSE}}}{\text{median}[p(\Sigma y)]}$ Right: $\hat{R}$ associated with the fit parameter $\Sigma$ . Both are shown for all 11 · 12 unbinned fits. The critical values that should not be exceeded are marked by dashed lines. . . . .	56
4.14	Posterior predictive check using the draws of the detector coefficients $a$ and $b$ for the kinematic bin $1250 \text{ MeV} \leq E_\gamma < 1310 \text{ MeV}, 0 \leq \cos \theta < 0.17$ . Points with error bars are the polarization weighted sum of event yields. The dashed line is the mean of the predictive values while the solid opaque lines are representative of one simulation draw $a^{(s)}, b^{(s)}$ . . . . .	57
4.15	Final results for the beam asymmetry $\Sigma$ in $\eta$ photoproduction off the proton for all kinematic bins obtained with BAYESIAN methods. They are compared with the results of a least squares fit and an unbinned fit as given in reference [Afz19]. All results agree within statistical error bars or within the widths of marginal posterior distributions. . . . .	59
4.16	Normalized residuals (left) and unaltered distribution (right) of all 10000 fits for the beam asymmetry $\Sigma = (1 - \delta) \cdot \Sigma_1 + \delta \cdot \Sigma_2$ . GAUSSIAN fits are performed with results given on top of each plot. . . . .	61
4.17	Normalized residuals (left) and unaltered distribution (right) of all 10000 fits for the background beam asymmetry $\Sigma_t^{\text{bkg}}$ . GAUSSIAN fits are performed with results given on top of each plot. . . . .	62
4.18	Fitted efficiency function (red line) applied to the polarization weighted sum of event yields (data points) for one toy Monte Carlo bin. 12 bins in $\phi$ are built for demonstration. . . . .	62
4.19	Combined (added) posteriors of all 1000 fits. Left: Signal beam asymmetry $\Sigma_1$ Right: Background beam asymmetry $\Sigma_t^{\text{bkg}}$ . A GAUSSIAN fit is performed with results given on top. . . . .	63
4.20	Combined (added) posteriors of all fits for the fit parameter $\Sigma_2^{\text{true}}$ . A GAUSSIAN fit is performed which reproduces exactly the values that were used for the simulations. . . . .	64
4.21	MCMC diagnostics for the event based BAYESIAN fit. Left: MCSE, Right: $\hat{R}$ -value. The critical values not to be exceeded are marked by the dashed lines. . . . .	65
4.22	Posterior predictive checks of one toy Monte Carlo bin using the draws from the marginal posteriors of the detector coefficients $a, b$ (opaque blue lines). The mean values are marked by the dashed line and follow the distribution of the data points which are the polarization weighted sum of event yields, using 12 $\phi$ bins. . . . .	65
4.23	Final results for the beam asymmetry $\Sigma$ in $\eta'$ photoproduction. Two sets of results are shown: The dark blue distributions and orange data points with errorbars are obtained with an unbinned fit that does not consider any background contributions. The light blue distributions and data points are obtained with the modified BAYESIAN fit and by correcting the point estimates according to Equation (4.42), respectively. All errors are statistical errors only. . . . .	67
4.24	Results for the additionally fitted $\Sigma_2^{\text{true}}$ (distributions) compared with the underlying data points [mahlbergphd] with statistical errors. The error bars on average cover $1\sigma$ of the distributions, indicating a successful fit. All errors are statistical errors only. . . . .	68
4.25	MCMC diagnostics for the event based BAYESIAN fit. Left: MCSE, Right: $\hat{R}$ -value. The critical values not to be exceeded are marked by the dashed lines. . . . .	69

4.26	Posterior predictive checks of the kinematic bin $1700 \text{ MeV} \leq E_\gamma < 1800 \text{ MeV}$ , $0.67 \leq \cos \theta < 1$ using the draws from the marginal posteriors of the detector coefficients $a, b$ (opaque blue lines). The mean values are marked by the dashed line and follow the distribution of the data points which are the polarization weighted sum of event yields, using 12 $\phi$ bins. . . . .	69
4.27	Final results for the beam asymmetry $\Sigma_{\eta'}$ for all energy and angular bins. Only the corrected results from the unbinned maximum likelihood fit and distributions from the modified BAYESIAN fit are shown. The bottom of each plot indicates the systematic error as gray bars. It was determined as previously discussed. . . . .	71
5.1	Results for the beam asymmetry $\Sigma_{\eta'}$ (orange errorbars and distributions) compared with the results for the energy bins $E_\gamma = 1569 \text{ MeV}$ , $E_\gamma = 1676 \text{ MeV}$ , $E_\gamma = 1729 \text{ MeV}$ reported in reference [Col+17] (black errorbars). Systematical errors are shown as grey bars. . . . .	74
5.2	Results for the beam asymmetry $\Sigma_{\eta'}$ (orange errorbars and distributions) compared with PWA solutions: etaMAID [Tia+18](dashed black line),. . . The errorbars only depict statistical error, the systematic error is shown as grey bars. . . . .	76



# List of Tables

---

1.1	Summary of the particles of the SM . . . . .	1
1.2	Allowed quantum numbers for the intermediate resonance state $N^*/\Delta^*$ . . . . .	4
3.1	The five most probable decay modes of the $\eta$ and $\eta'$ meson. The most probable further decay with according branching ratio is shown in brackets.[Wor+22] . . . . .	11
3.2	Examined MC reactions that were used in sum for the fit . . . . .	17
3.3	Fit functions and cut ranges for each kinematic variable . . . . .	18
3.4	Total cross sections $\sigma$ in the energy range 1500 to 1800 MeV, branching ratios (BR) to $n\gamma$ final states, maximum acceptance $\tilde{A}$ for signal and possible background contributions as well as the expected signal to background ratio $R$ . References [2pi0_cs] and [pi0eta_cs] give the cross sections only up to roughly 1500 MeV, the given values are thus upper bounds. For the same reason, from reference [3pi0cs] only a lower bound can be estimated. For all other reactions a rough mean over the energy bins of interest is built. If the references provide only differential cross sections a crude integration in each angular bin is performed. In case only very few ( $O(10^1)$ ) decays pass event selection, the acceptance is built in one global bin only for the respective reactions. This is indicated by the horizontal line. . . . .	26
3.5	Relative loss in signal and background events if a cut on $\Delta E$ is applied. . . . .	34
4.1	Summary of the complete setting of all toy Monte Carlo experiments for the event based fit. Values and table layout adapted from [Afz19]. . . . .	49
4.2	Summary of the complete setting of all toy Monte Carlo experiments for the event based fit. Table layout adapted from [Afz19]. . . . .	60